

DETERMINING FRICTION COEFFICIENTS FOR INTERRILL FLOWS: THE SIGNIFICANCE OF FLOW FILAMENTS AND BACKWATER EFFECTS

DAVID L. DUNKERLEY*

School of Geography and Environmental Science, PO Box 11A, Monash University, Victoria 3800, Australia

Received 7 February 2002; Revised 30 June 2002; Accepted 6 September 2002

ABSTRACT

Friction coefficients in overland flows are customarily estimated from mean flow properties (depth, velocity, slope) that subsume spatial variations in flow arising from two major causes: microtopography and obstacles. This paper uses laboratory experiments in shallow flumes to examine the extent of non-uniformity in flow conditions associated with each cause. Randomly placed emergent obstacles in a flume with a shallow axial channel generally yielded higher hydraulic roughness than the same pattern of obstacles on a planar flume, as well as greater variation in roughness as the obstacle locations were altered. In both flumes, hydraulic roughness fell with increasing Reynolds number for 10% obstacle cover, showed a flattening trend at 20% cover, and exhibited a convex-downward trend at 30% obstacle cover. These results indicate the progressive onset of flow controls at narrow gaps in the obstacle field. In such flows, the use of mean flow properties conceals the existence of two main subdivisions of flow: flow filaments and backwater flows. In the experiments, flow filaments involved velocities more than twice the overall mean, whereas backwater flows were much slower than the mean. The existence of fast-moving flow filaments may be significant in understanding soil transport in surface runoff, and backwater depths may modify splash detachment. Similarly, friction coefficients that fail to reflect these important non-uniform flow components may not be optimal for hydraulic calculations or in erosion models. It is concluded that new approaches to observing and processing flow data may be required, in order to avoid the loss of important flow detail that is entailed in assuming uniform flow conditions. Copyright © 2003 John Wiley & Sons, Ltd.

KEY WORDS: friction coefficient; flow filament; backwater effects; surface runoff; non-uniform flow

INTRODUCTION

This paper considers some of the determinants of friction coefficients in shallow overland flows that are related to non-uniformity of flow properties. Friction coefficients in overland flows need to be understood so that the behaviour of surface runoff – especially the controls on its velocity, erosivity and sediment-carrying capacity – can be systematically understood. Appropriate values for friction coefficients are also required as inputs for small-scale hydrologic and runoff modelling.

Friction coefficients are influenced by a complex range of factors. In addition to the grain and form resistance arising from the mineral soil surface itself, there are several other influences. Microtopography, with an amplitude of millimetres to centimetres, is generally present even on slopes that appear relatively uniform and smoothly sloping. This produces preferred flow pathways and filaments of deeper and faster overland flow, as demonstrated by dye tracing in the classical field experiments by Emmett (1970). Emmett (1970) pointed out that the existence of flow filaments does not mean that the rest of the surface carries no flow. Rather, the faster filaments generally lie within an extensive flowing sheet of water. The hydraulics of both the flow filaments and the remaining non-filament flow affect the value of the friction coefficient for the surface flow as a whole (hereafter termed the *flow field*). Another contributor to the friction coefficient is obstacle resistance arising from the presence of loose or partly embedded stones, organic litter or crop residues, or the stems of grasses or other plants. Typically, some such obstacles will lie in the path of flow

* Correspondence to: Dr D. L. Dunkerley, School of Geography & Environmental Science, PO Box 11A, Monash University, Victoria 3800, Australia. E-mail: david.dunkerley@arts.monash.edu.au

filaments, while others will lie in non-filament flows. There are subsidiary effects on flow caused by obstacles. These include the upward displacement of flow depths that correspond to the submerged volume of obstacles (Dunkerley, 2002a, 2003), depth variations related to surface tension and meniscus formation along their edges (Dunkerley, 2002b), and acceleration of flow on preferred flow paths between them. It has been shown that, under certain conditions, protruding obstacles may increase mean flow velocities and reduce effective friction coefficients in comparison with a similar but obstacle-free soil surface (Abrahams *et al.*, 2000; Dunkerley *et al.*, 2001).

Despite the likelihood that this range of influences results in significant internal variability of flow properties in surface runoff, such as marked local variation in depths and velocities, it has been customary to describe surface runoff in terms of mean values derived for the entire flow field (i.e. filaments and non-filament flows taken together). This was the approach adopted originally by Emmett (1970) and by others cited below. In particular, to derive a value for the widely used Darcy–Weisbach friction coefficient f , the depth d , velocity v and energy slope S terms in Equation (1), in which g is the acceleration due to gravity, are commonly taken to be means for the entire flow. This amounts to an assumption that the flow is two-dimensional and uniform.

$$f = \frac{8gdS}{v^2} \quad (1)$$

This paper considers the consequences of this presumption of uniform flow. Laboratory experiments are used to derive data on flows with and without microtopography, and with and without obstacles simulating surface stones. The objective is to explore the internal variability in hydraulic conditions within these flows, to focus attention on the depth and velocity variations that occur in filament and non-filament zones, and hence to assess the validity and usefulness of friction coefficients based on mean values of flow properties.

The application of uniform flow formulae to complex surface runoff

Friction coefficients have been derived for natural rangeland surfaces (Emmett, 1970; Dunne and Dietrich, 1980; Roels, 1984; Abrahams *et al.*, 1986; Weltz *et al.*, 1992) as well in flumes carrying varying amounts of stones, crop residues, or other sources of flow resistance (Gilley *et al.*, 1991, 1992; Rauws, 1988; Barros and Colello, 2001). In these studies, the use of flow-field means has been adopted.

An important consideration is how the input data needed for the use of a relation such as Equation (1) are collected. Frequently, only sufficient variables are measured to allow a mean value for the remaining unknown to be found. For example, if discharge Q is imposed (by pumps, constant-head tank, etc.), flow width w is fixed (by plot or flume side walls) and depth d has been measured at sufficient points in the flow, then mean velocity can be found using $v = Q/wd$. Alternatively, if Q and w are fixed and v is measured (by dye timing, etc.) then one can find depth using $d = Q/wv$. When the entire cross-section is not submerged by the flow (e.g. when protruding stones or microtopographic high-points are still emergent), then it is conventional either to estimate an effective flow depth d' from $d' = Q/wv$, where w is the whole width of the surface traversed by the flow (Barros and Colello, 2001), or else to estimate an effective width by reducing the total width by the fraction that remains emergent (Abrahams and Parsons, 1990).

These procedures rely on the assumption that the flow is uniform or reasonably so, such that mean properties derived in the ways reviewed adequately represent the flow properties being studied. For this to be strictly the case, the mean flow depth and mean velocity must remain constant in the flow field (Henderson, 1966). Whether this condition is met becomes of additional concern when mean flow properties are used to estimate a friction coefficient using Equation (1), since the derivation of this relation itself only holds for uniform flow (see Dunkerley (2002a) for further comments).

The role of preferred flow paths (flow filaments) and of hydraulic flow controls

Preferred flow paths (hereafter termed *flow filaments*) are those tracks along which flows move more rapidly than on the adjacent soil surface. As described by Emmett (1970), they follow low-lying paths bordered by features like higher parts of the soil surface, shrub mounds, and outcropping rock. The funnelling of runoff from surrounding soils into these paths results in greater depths and faster flow velocities along them. Because

of the concentrated flows that are carried along flow filaments, a narrowing of a flow path may result in the creation of a choke or flow control unable to conduct all of the arriving flow. The term 'control' is used in the sense of a feature of the flow path that determines a depth–discharge relationship past the feature (Henderson, 1966: 41). In such a case, where there is a limited ability for a gap to carry the whole flow arriving in the flow filament without some kind of dynamic adjustment to flow depths to reach a balance between arriving and departing flows, an impounded body of water (hereafter termed a *backwater*) is created. This is an accumulation of deeper water upstream of the flow control. This backwater zone would exhibit both an increase in depth and a decrease in flow velocity in comparison with conditions that would exist if the control was removed. Recalling the form of Equation (1), it is evident that flow properties (depth or velocity) assessed in backwater zones will result in elevated values of f , since d (which is increased in backwaters) is in the numerator and v^2 (which is reduced in backwaters) is in the denominator. On the contrary, if measurements are made in the vicinity of flows passing through a control, where v will be increased and d reduced as flows move toward the critical condition, then a much lower value of f would result.

Flow filaments can also be created on a small scale by surface obstacles like stones and organic detritus, even on a planar surface. In this case, the preferred flow paths follow a track constrained by the geometric layout and spacing of the obstacles. Stones lying closely adjacent in the path of a flow filament can create a flow control and a local backwater. Such small backwaters, located across the surface, are probably a significant contributor to detention storage.

In flows containing flow filaments and backwaters, observations of flow depth cannot be converted into local estimates of velocity, since the flow might be free-flowing or in a zone of backwater detention. Likewise, dye timing over flow paths of significant length cannot readily be associated with a point reading of the flow depth to resolve this uncertainty. A method for observing virtual 'point' velocities is thus required, to be used as an adjunct to flow depth readings. Such a method is introduced below.

EXPERIMENTAL METHODS

A new system for measuring flow velocities

The new method, which is described in detail elsewhere (Dunkerley, in press), uses two small optical sensors mounted above the flow and separated by 10 mm in the direction of flow. A floating reflector disc made of aluminium foil, 10 mm in diameter, is released just upstream and is carried on the water surface by surface tension. In passing beneath the upstream sensor, the reflector triggers a 'start' pulse, and shortly thereafter a 'stop' pulse as it passes beneath the downstream sensor. These signals operate a timing device similar to a stopwatch but providing millisecond resolution. Testing indicates that the device records virtual 'spot' readings of surface velocity, the same parameter measured with dye timing. The results are highly repeatable and can be gathered at many points along a flow filament. This device allows the gathering of velocity data that do not depend on measured flow depths.

The new flow velocity sensor was used in combination with a computer-controlled needle gauge and *XY* gantry system previously developed by Dunkerley *et al.* (2001). In combination, these devices permit the determination of flow depth and surface velocity within the surface runoff sheet, and these paired data can readily distinguish deep but slow (backwater) flow from shallower but faster (filament) flows. That is, the paired measurements allow the explicit recognition and measurement of non-uniform flows.

The overland flow flumes

Experiments were conducted to simulate non-uniform flows across a dryland surface carrying a cover of scattered stones. Two shallow interrill flow boards were constructed by roughening boards 600 mm wide and 2400 mm long with medium sand applied to wet varnish. Sidewalls were attached to form a shallow channel. The bed of one (the *flat board*) flume was made as flat as could be achieved with the hand-application of sand to the varnish, whereas the other (the *channel board*) included a channel 10 cm wide and 2 mm deep. This was made by applying additional coats of varnish and sand to the left- and right-hand sides of the flume (Figure 1), leaving a slightly lower central channel that was not re-coated. During runoff experiments, flumes were inclined at a fixed slope of 1.2° and water was recirculated along them at nine flow rates (10,

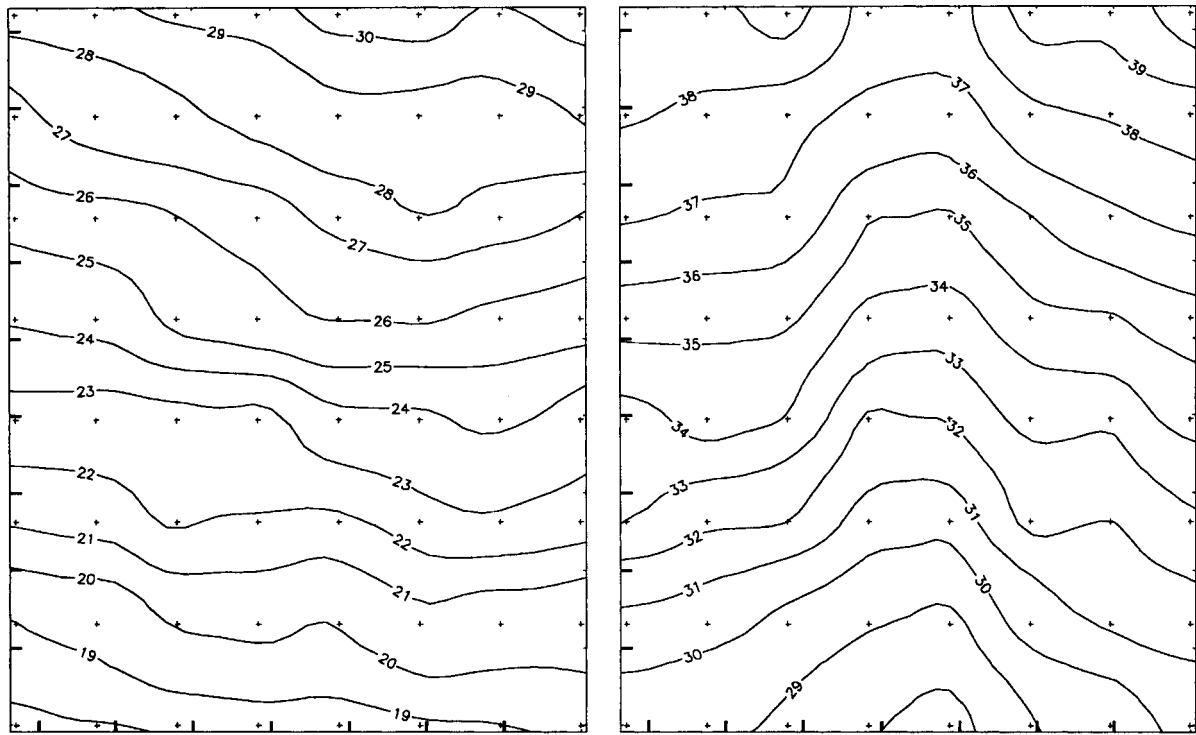


Figure 1. Contour plots of the flat and channel boards. Contour interval is 1 mm. Datum is arbitrary elevation near lower end of flume. The small crosses indicate the points used for measurement of flow depths. Small ticks in the graph frames are at 5 cm spacing

20, 30, 40, 50, 60, 70, 80 and $90 \text{ cm}^3 \text{ s}^{-1}$) by peristaltic pumps. On each flume, stones were represented by blocks of brass 46 mm square and 20 mm thick, which were never overtopped by the flow. Five different obstacle arrangements, referred to as layouts A–E, were developed using random numbers to form X and Y coordinates (Figure 2), and these same arrangements were tested on each flume at the nine different flow rates. This procedure was repeated for cover fractions of 10, 20 and 30%, set out using parts of the sequence of random coordinates as required; in addition, the friction coefficient for each flume was determined using the same sequence of flow rates, but with no obstacles in place. All measurements were made in a central $0.5 \text{ m} \times 0.5 \text{ m}$ area of each flume, in order to minimize any disturbing effects arising near the lower lip of the flume, or near the top of the flume where the feed water was delivered from a perforated pipe. The layouts A–E were set out in this central measurement area. Additional obstacles were employed both upstream and downstream in order to keep the same level of obstacle drag along the whole length of the flume. The measuring gantry was used to measure flow depths to the nearest $25 \text{ }\mu\text{m}$ at 64 points located on an 8×8 grid covering the central measurement area. The optical velocity measuring device (tachometer) described previously was used to make spot measurements of velocity at various locations, also within the central test area. These were selected to include both flow-filament and backwater areas, as explained later. All such readings, wherever taken within the flume, were repeated five times at the same location and the mean determined. The tachometer was rigidly mounted above the flow during this process to ensure that the same location within the flow field was observed in each replicate measurement. Dye timing was carried out periodically using marked 50 cm flow paths (top to bottom of the central test area) in order to determine mean velocities along the flumes, injections of 0.2 ml of fluorescein dye being used. As for the tachometer observations, all dye timings were repeated five times along the same track and the mean taken. Water temperatures were monitored regularly using a platinum resistance thermometer, allowing viscosity to be calculated from polynomial relationships set out by Weast (1979).

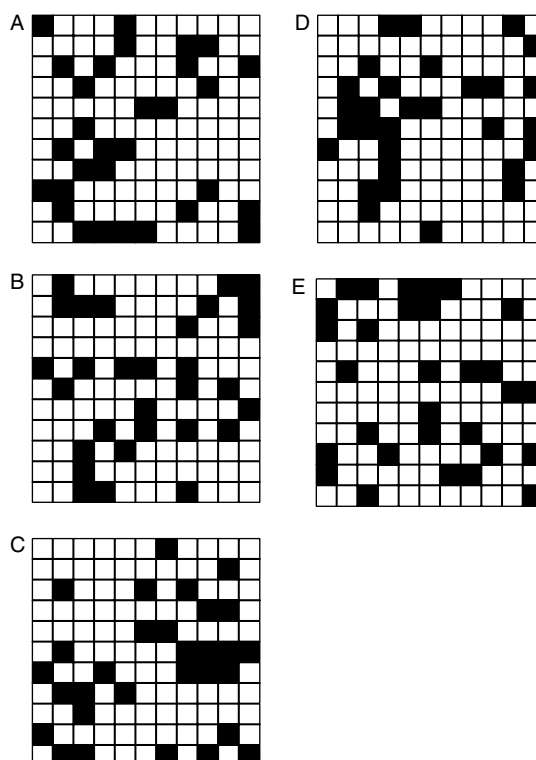


Figure 2. The five random patterns of obstacle layout (30% cover). The 10 and 20% cover fractions were subsets of the positions shown

The resulting data permitted the flow-field mean velocity and depth to be computed, but also allowed the local depth, velocity, Reynolds number, Froude number and Darcy–Weisbach f to be derived for selected locations lying on flow filaments or in backwater areas.

Several supplementary experiments were conducted on a simpler layout of obstacles, arranged to form a barrier one obstacle in width across the middle section of the flat board. At the centre of this barrier, a gap of 95 mm width was left in order to form a simple flow control. The behaviour of depth and velocity within, upstream and downstream of this control were investigated using the measuring gantry and optical tachometer at four imposed flow rates of 20, 40, 60, and 80 cm³ s⁻¹. These tests were made in order to be able to study the flow conditions in a gap or flow control having simple geometry. In the random obstacle fields, many of the controls carried flow passing obliquely and having significant curvature of flow paths. The objective of the simple gap measurements was to examine velocities, depths, and Froude numbers (in relation to the achievement of critical flow) at a control.

In processing the data, the following relations for Reynolds number

$$\text{Re} = \frac{4vd}{\nu} \quad (2)$$

and Froude number

$$F = \frac{v}{\sqrt{gd}} \quad (3)$$

were adopted, where d (cm) is the mean flow depth, v is the mean flow velocity (cm s⁻¹), and ν (cm² s⁻¹) is the kinematic viscosity.

Table I. Summary of flow characteristics for the flat and channel boards for all test conditions, including the obstacle-free flumes and obstacle cover fractions of 10, 20 and 30%. The range of flow properties is shown for imposed discharges in the range $10\text{--}90\text{ cm}^3\text{ s}^{-1}$

Obstacle cover fraction	Flat board					Channel board				
	Mean flow depth (mm)	Mean flow velocity (cm s^{-1})	f	F	Re	Mean flow depth (mm)	Mean flow velocity (cm s^{-1})	f	F	Re
Nil (bare flume)	0.81–1.71	2.50–10.50	0.28–2.29	0.28–0.81	75–687	0.73–1.59	2.76–10.06	0.26–1.57	0.33–0.81	80–612
10%	0.89–2.19	2.51–9.22	0.44–2.41	0.27–0.63	85–774	0.84–1.97	2.66–10.15	0.32–1.95	0.29–0.73	88–797
20%	0.81–2.72	3.10–8.38	0.73–1.57	0.35–0.52	95–866	0.88–2.80	2.86–8.06	0.71–1.79	0.31–0.50	94–861
30%	0.98–4.36	2.91–6.03	2.09–2.33	0.29–0.30	108–989	0.94–6.38	3.07–6.38	1.69–1.79	0.32–0.37	108–987

RESULTS

In total, the nearly 300 flow experiments made in the flumes spanned a wide range of flow conditions, and involved $>20\,000$ bed elevation and depth measurements. Flow-field properties were generally laminar and sub-critical (Table I), though, at the higher flow rates, injected dye confirmed that there were turbulent regions at some locations on the flume surface. Flow depths were generally <10 mm. Mean flow conditions are noted below for the various obstacle cover treatments. The data are not fully explored here, and only key aspects of the results relevant to the objectives of this paper are highlighted. Attention is particularly focused on the variation of friction coefficient with obstacle layout and with Re, and on the velocity and depth in flow filaments and backwater flows.

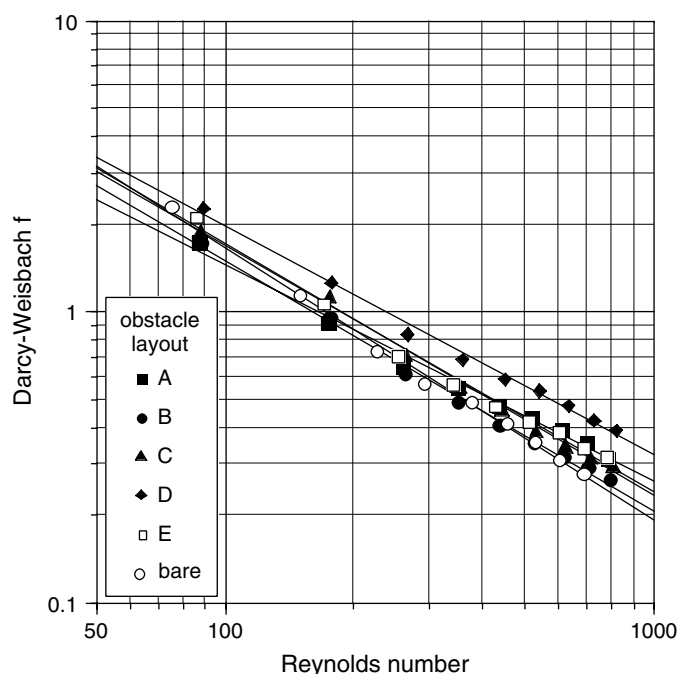


Figure 3. Relationships of f –Re for the bare flat board and for the 10% obstacle covers. The fitted lines are power-function regressions detailed in Table II

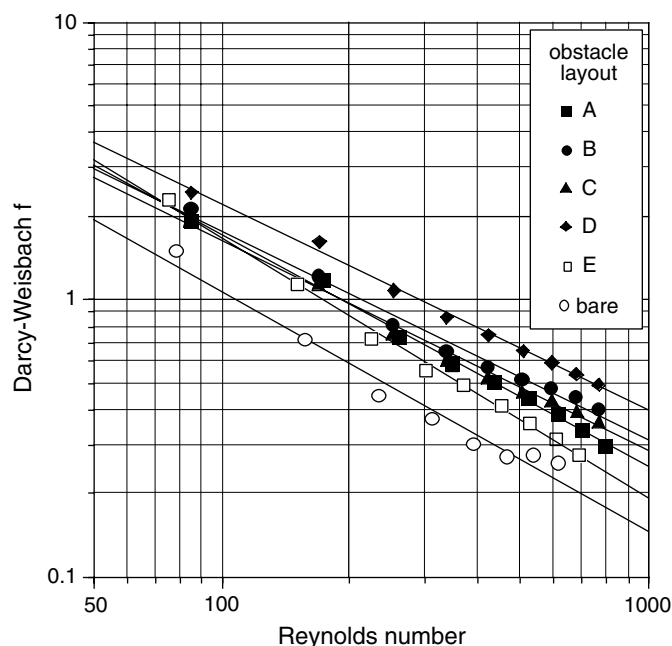


Figure 4. Relationships of f - Re for the bare channel board and for the 10% obstacle covers. The fitted lines are power-function regressions detailed in Table II

Table II. Regression models for the f - Re relations for the 0% and 10% obstacle covers on the flat and channel boards, listed separately for the five geometric obstacle layouts (denoted A-E). All relations of the form $f = aRe^b$, and each is statistically significant ($p < 0.0001$). Correlation coefficients are listed for each relationship

Flume obstacle layout	Flat board			Channel board		
	a	b	r^2	a	b	r^2
Bare	124.6	-0.938	0.996	57.1	-0.865	0.967
A	44.2	-0.743	0.991	80.4	-0.836	0.996
B	78.6	-0.860	0.996	54.8	-0.747	0.998
C	92.4	-0.866	0.996	52.8	-0.756	0.992
D	71.9	-0.782	0.994	67.8	-0.743	0.996
E	83.7	-0.847	0.990	104.3	-0.772	0.986

Bare flume and 10% obstacle cover

On the bare flumes, the relation between f and Re exhibited the negatively sloping power function relationship classically exhibited on the Moody diagram, being fitted by statistically significant relations (Figures 3 and 4, Table II).

On the channel board, the relation began to change at $Q = 50 \text{ cm}^3 \text{ s}^{-1}$ ($Re = 470$), with the slope of the f - Re relation flattening as Q increased. This probably reflects the increasing incidence of turbulent conditions, and greater viscous energy dissipation within the flow, owing to the concentration of flow within the channel. No comparable upward bending of the f - Re relation was exhibited on the flat board, where the data were tightly fitted by a relation having the slope of -0.94 , close to the smooth-surface value of -1.0 expected for laminar flows. If the lower four flow rates alone are fitted for the channel board, then the linear model exhibits a slope (-0.94) identical to that of the flat board.

For the 10% obstacle covers, the f - Re relations on both flat and channel boards were likewise well fitted by power-function relations that plot as straight lines on the log-log Moody relation (Table I and Figures 3 and 4). The upward curvature seen on the bare channel board was no longer evident, owing to the partial obstruction of the channel and the obstacle drag. For the flat board, the f - Re slope was reduced to -0.82 ; this reduced to -0.79 on the channel board. These slopes are significantly different from -1 (small-sample t -test, Freund, 1974).

Hydraulic roughness f averaged across all five obstacle layouts was slightly higher on the channel board at all flow rates. On both boards, obstacle layout D yielded the highest value of f , and layout E the lowest f (flat board) or second-lowest (channel board). Among the five layouts at the highest imposed flow rate on the flat board, $0.264 < f < 0.391$, the maximum f being 48% larger than the minimum. For the channel board the corresponding range was $0.29 < f < 0.64$, the maximum being 120% larger than the minimum.

20% obstacle cover

For this cover treatment, both flat and channel board f - Re relations show significant departures from linearity, flattening at higher flow rates, and with an upward trend on the channel board at flows of 80 and 90 $\text{cm}^3 \text{s}^{-1}$ (Figures 5 and 6). Roughness averaged across all five obstacle layouts was very slightly higher on the flat board at all flow rates except the lowest, where roughness was greater on the channel board. The variation in f across layouts A-E is larger for the flat board. As for the 10% cover, layout D yields the highest f on flat and channel boards and layout E the lowest on the flat board. For the channel board, layouts B and C yield closely similar values of f that are the minimum on that board. Among the five layouts at the highest imposed flow rate on the flat board, $0.104 < f < 0.441$, a range of 324%. For the channel board, the range was $0.594 < f < 0.894$, or 51%.

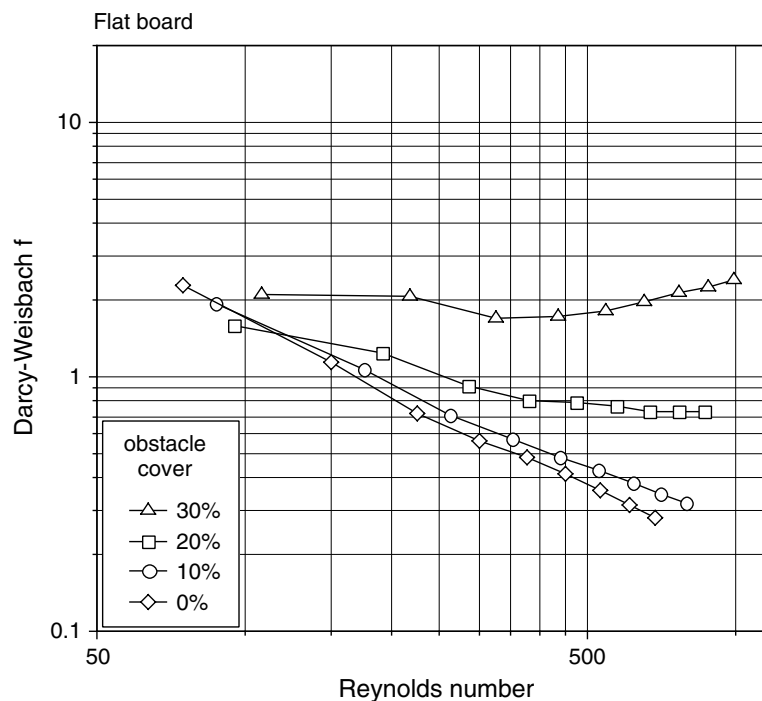


Figure 5. Plot of f - Re relationships for bare, 10%, 20% and 30% cover treatments on the flat board. The relationships are indicated as line graphs

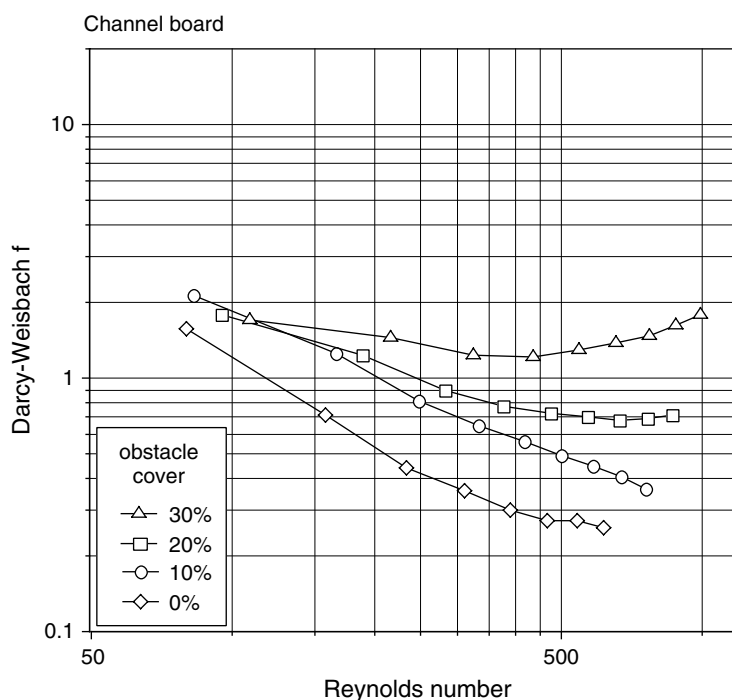


Figure 6. Plot of f - Re relationships for bare, 10%, 20% and 30% cover treatments on the channel board. The relationships are indicated as line graphs

30% obstacle cover

For the highest obstacle cover tested, the tendency toward increasing non-linearity of f - Re relations is continued, with the curves being concave upward for both boards (Figures 5 and 6). At all flow rates, roughness was considerably higher on the flat board than on the channel board. On the flat board, the positive slope commences at about $Q = 30 \text{ cm}^3 \text{ s}^{-1}$ (at $Re = 300$); on the channel board, this occurs at about $Q = 40 \text{ cm}^3 \text{ s}^{-1}$ ($Re = 450$). For each board, layout A resulted in the highest f values, supplanting layout D, which yielded the highest f for both 10% and 20% covers. Once again, layout E yielded the lowest f on the channel board and second-lowest on the flat board. Among the five layouts at the highest imposed flow rate on the flat board, $1.301 < f < 3.927$, a range of 202%. For the channel board, the range was $0.967 < f < 2.861$, a spread of 196%.

Comparing flow-field velocities with optical tachometer 'spot' readings

The mean flow velocities in Table I were derived from the grids of flow depth observations using the relation $v = Q/wd$, with w being reduced in proportion to the cover fraction of emergent obstacles. These are analyses made in the conventional way, on the presumption that uniform flow conditions were approximated during the tests. They can be compared with the virtual 'spot' readings made with the tachometer and with data collected using conventional dye timing.

Consider the 30% cover in layout A (highest f) on the flat board at $Q = 80 \text{ cm}^3 \text{ s}^{-1}$. This is in the region of strong upward curvature of the f - Re relation (Figure 6). Flow filaments were clearly evident in the flow field, and were delineated using dye injections. Dye timing of flow through the full length of the preferred flow paths down the left- and right-hand sides of the board (Figure 7) yielded mean surface velocities of 14.8 cm s^{-1} and 17.8 cm s^{-1} respectively. These velocities were calculated along the measured lengths of the sinuous flow paths, which were 90 cm and 53 cm respectively, and not the straight-line downslope path across the test area of 50 cm. There is some uncertainty attached to these values, since the flow paths were sketched approximately by hand on the basis of dye trajectories prior to being digitized, and so may

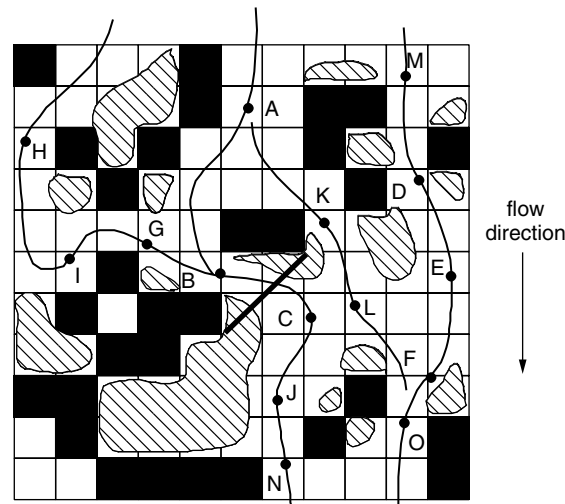


Figure 7. Diagram showing the locations of flow filaments and of optical tachometer measurements of filament speeds in obstacle layout A, 30% cover on the flat board. The positions of backwater flow zones are also marked. The obstacle layout is the same as that shown in Figure 2. The line crossing the filament between sample points B and C is the location of the depth measurements shown in Figure 8

not be exact. More reliable optical tachometer velocity observations were made at 15 points along these flow paths (Figure 7). The arithmetic mean for the left-hand side path is 17.5 cm s^{-1} and for the right-hand side it is 18.3 cm s^{-1} . Given that the two methods measure flow velocity at differing locations (the dye integrating a mean over a 50 cm path, and the tachometer a much more local value measured over a 10 mm path), these results seem accordant. (Because of their differing scales of operation, matched data taken at precisely the same location using the two techniques, and which could be more rigorously compared, cannot be obtained.) Adjusting surface velocities to profile means using the conversion $v = \alpha v_{\text{surf}}$ with $\alpha = 0.56$ (Dunkerley, 2001) yields a profile-mean flow velocity along these filaments of about 10.0 cm s^{-1} . This can be compared with the flow-field mean velocity, based on 40 depth measurements, of 4.83 cm s^{-1} . Thus, the filament flows involve mean velocities that are about twice the flow-field mean. For the channel board under the same conditions, the flow-field mean velocity was 5.21 cm s^{-1} . Once again, the tachometer 'spot' readings of surface velocity showed much faster filaments with the flow, the highest measured being 20.2 cm s^{-1} , equivalent to a profile mean of 11.3 cm s^{-1} . This is again more than twice the flow-field mean. For layout E on the channel board, which yielded the lowest f , tachometer velocities reached 23.8 cm s^{-1} , or a profile mean of 13.3 cm s^{-1} . This again exceeds the flow-field mean of 7.46 cm s^{-1} , but only by about 1.8 times.

The tachometer velocities recorded along the separate flow filaments (Figure 7 and Table III) show that although the filament velocities remain higher than the flow-field mean for the whole of their path through the obstacle field, there is significant longitudinal velocity variation within a filament. Velocities tend to be greatest in and close to narrow gaps (flow controls) and slower in more open areas of the obstacle field. The rapid surface velocity reached in the flow control at location N (28.7 cm s^{-1}) is noteworthy, since this corresponds to a profile mean of at least 16 cm s^{-1} , which is more than three times the flow-field mean.

Backwater areas were developed at many locations upstream of flow controls within the obstacle fields. The deeper flow within them could readily be seen, and attempts to measure velocities in these areas showed very sluggish flow. Indeed, injections of dye or released optical tachometer targets drifted very slowly, often remaining for many seconds almost without movement, or drifting seemingly at random, until finally being drawn into a flow filament and rapidly accelerating. This prevented consistent and reliable measurement of velocities in these areas. Nevertheless, the failure of dye or tachometer targets to move for several seconds made it clear that velocities were in many cases $\ll 1 \text{ cm s}^{-1}$. The demonstrated high filament flow velocities in any case require that there also be slow-moving areas in order to reduce the flow-field mean velocities

Table III. Surface speeds along flow filaments on flat board carrying 30% obstacle cover in layout A (see text for details). Speeds were measured across a 10 mm flow path using an optical tachometer. Each value is the mean of five replicate measurements

Measurement point	Surface flow velocity (cm s ⁻¹)		Flow depth (mm)
	Mean	Standard deviation	
A	22.3	2.01	4.48
B	25.0	1.15	6.20
C	21.4	2.45	6.28
D	25.6	1.42	4.20
E	19.1	1.79	5.75
F	8.4	1.79	8.85
G	18.1	3.74	7.53
H	15.9	0.75	6.25
I	8.8	2.55	9.25
J	15.9	2.57	6.83
K	12.5	3.34	3.28
L	18.1	3.51	5.75
M	16.9	1.39	5.45
N	28.7	5.01	2.7
O	21.6	1.75	5.9

to 4.83 cm s⁻¹ (flat board) and 7.86 cm s⁻¹ (channel board). Given that the flow filament velocities were 10–13 cm s⁻¹, then the backwater areas must have carried very slow flow to reduce the mean velocity to this extent. In summary, the mean flow-field velocities based upon the depth measurements lie above the actual speed in many of the backwater areas and below that of the velocities recorded along the flow filaments.

A set of closely spaced depth observations in a transect spanning the filament flow on the flat board with a 30% obstacle cover in layout A was made at the location marked on Figure 7, between observation points B and C. Depth was recorded using the gantry at 1 cm spacings on a line crossing this flow filament at right angles. The results (Figure 8) show that the flow is shallowest along the axis of the flow filament, averaging 4.5 mm, and deeper on its flanks. Along this section, the axis of the filament was nearly 1.5 mm (or about 30%) shallower than the flanking, non-filament flow. To judge from the zone where depths were reduced, the width of the shallower filament was about 6 cm. Taking the surface flow speed at the cross-section to be the average of observation points B (just upstream) and C (just downstream) of the cross-section yields an estimate of 23.2 cm s⁻¹ for surface speed, or a profile mean of 13 cm s⁻¹. Thus, the discharge passing through the axial zone of this filament is about (6 × 13 × 0.45) or 35 cm³ s⁻¹. Thus, 44% of the flow passes through only 17% of the flume width, confirming that the flow filament is an area of significant flow concentration.

Differences in the distribution of flow depths among the obstacle layouts

The flow depth data obtained using the gantry are precise and do not depend on assumptions of flow behaviour. This is in contrast to the flow-field mean velocities, which evidently lie somewhere between those of filament and backwater flows.

The distribution of flow depths can, therefore, be taken as a measure of the extent of backwater effects. From what has just been presented, in the range of flow rates where the f -Re curves have positive slope, deep zones are probably located away from flow filaments, primarily where backwater effects above flow controls detain flow. Shallower flow depths represent either flow filaments or, where the obstacle layout is more open or the imposed flow lower, flows not significantly constrained by flow controls.

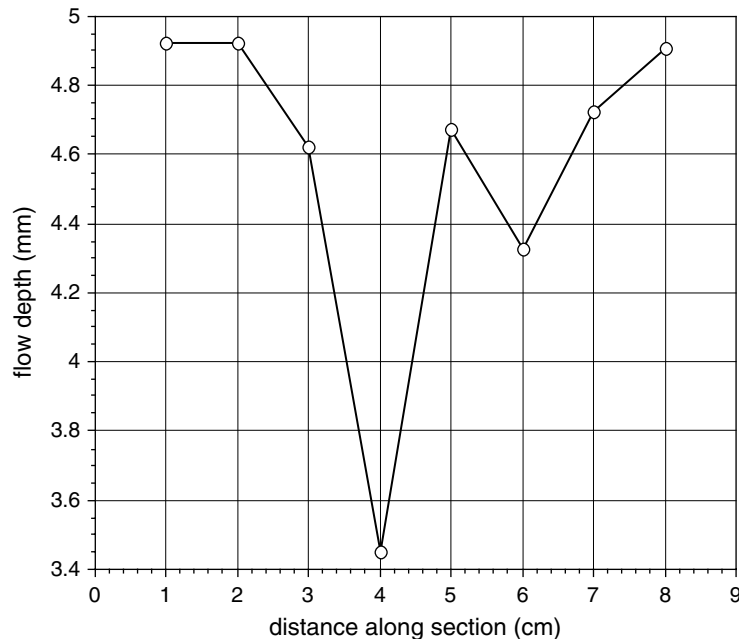


Figure 8. Cross-section of flow depths on a flow filament from obstacle layout A, 30% cover on the flat board. The location of this cross-section is marked on Figure 7

Results from the flat and channel boards at the highest imposed flow rate ($Q = 90 \text{ cm}^3 \text{ s}^{-1}$; Figure 9) illustrate this. The 30% obstacle cover E on the channel board, which yielded the lowest f , has a mean depth of 3.07 mm, whereas layout A gave the highest f and had a mean depth of 4.39 mm. This is a 43% increase in flow depth for the same cover fraction and flow rate, attributable to the geometric arrangement of the obstacles. Similarly, the 30% obstacle cover B on the flat board gave the lowest f , with a mean depth of 3.34 mm, and maximum f for layout A, with a mean depth of 4.73 mm. This is a 41.6% increase in flow depth for the same cover fraction and flow rate. The frequency distributions of flow depths in these four cases (Figure 9) show a change from being positively skewed for the lowest roughness obstacle layouts to being more symmetrical, with the modal class at higher depth, for the highest roughness obstacle layouts. Given that flow filaments are shallower than their flanking flows, the bulk of the increased depths found in layout E must be in backwater areas.

The tests with a geometrically simple, single control

The experiments made with a single gap in a line of obstacles demonstrated clearly what happens in the vicinity of a simple control. An influence on flow depth, creating an extensive backwater region, extended more than 20 cm upstream of the control. Through this distance, the flow progressively deepened toward the control. At 5 cm above the control, the flow was more than 4 mm deeper than at the upstream end of the backwater. Just above the control, the depth was drawn down as flow accelerated through the control. The mean flow depth across the full width of the flat board with the control in place was determined 50 mm upstream of the control using the gantry system to record depths at five evenly spaced points. For $Q = 80 \text{ cm}^3 \text{ s}^{-1}$ this yielded a mean depth of 6.1 mm. At the mid-point of the control, which was 50 mm long in the flow direction, the depth had fallen to 4.5 mm. Tachometer measurements of the flow velocities establish the rapid acceleration of flow approaching and passing through the control. For instance, for $Q = 80 \text{ cm}^3 \text{ s}^{-1}$, the mean surface velocity 10 cm above the control was 2.4 cm s^{-1} . By 5 cm above the gap this had accelerated to 6.1 cm s^{-1} , and at half-way through the control, on its centreline, the velocity reached 26.9 cm s^{-1} . Thus, flow through the control was more than ten times faster than that 10 cm upstream in the backwater area. Similar acceleration was recorded for the three lower flow rates also. At the mid-point of the control the

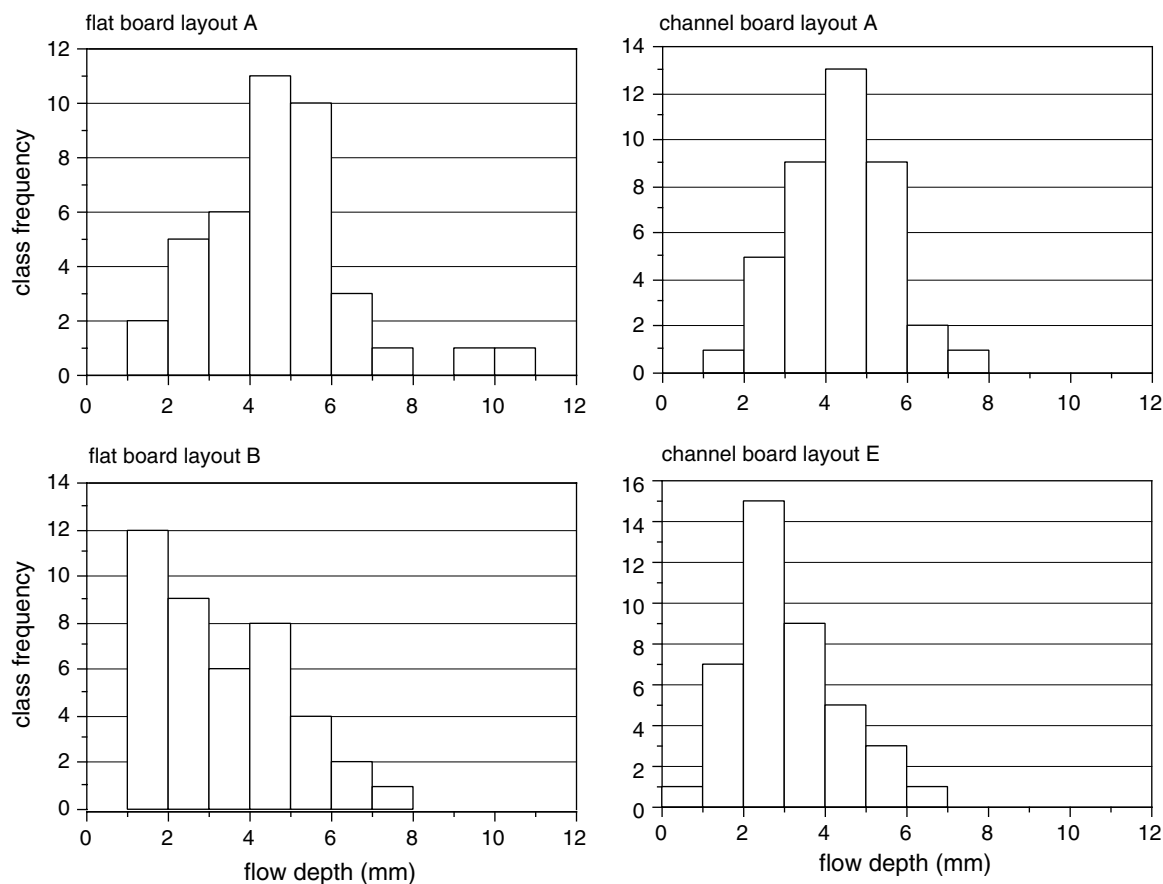


Figure 9. Frequency distributions of flow depth for layout A (highest f) and layouts B (lowest f , flat board) and E (lowest f , channel board) at $Q = 90 \text{ cm}^3 \text{ s}^{-1}$

$80 \text{ cm}^3 \text{ s}^{-1}$ data yield $Re = 950$, whereas for the backwater flow 5–10 cm upstream, $Re = 150$. Using the same data, the Froude number is 0.06 in the backwater 10 cm above the control. This rises to 1.03, confirming the presence of critical flow, at the mid-point of the control. If the depth and velocity data (converted to profile means using $\alpha = 0.56$) are used to calculate a friction coefficient from Equation (1), then for the backwater flows (deep, slow) the result is $f = 40.9$ and for the flow filament at the control (shallow, fast) it is $f = 0.16$.

DISCUSSION

For a given imposed flow rate, there is a wide range of friction coefficients among the five obstacle layouts at each cover fraction. At the highest imposed flow rates, the highest f was typically two to three times that of the lowest. This demonstrates that the use of a simple cover fraction as a basis for the prediction of friction coefficients is unlikely to be successful. More importantly, the variation in f with obstacle layout sheds light on the processes that determine the value of f .

The form of the f – Re relations (Figures 3–6) provides key evidence. For the 10% obstacle cover, the relations show the same negatively sloping, linear form as do the bare flat and channel boards. Thus, when the obstacles do not greatly obstruct the passage of flow down the board, the form of relationship between f and Re is unaffected. On the flat board, the value of f for any Re is likewise hardly affected by the presence of the 10% obstacle cover. There is a larger increase on the channel board, where the axial concentration of flow in effect delivers a higher flow intensity to the field of obstacles lying within the channel. In contrast,

when obstacle cover is 20%, the f -Re relations begin to flatten at the highest six flow rates on both boards. Indeed, on the channel board the two highest flow rates are associated with a slight upward curvature in the f -Re plot. Finally, at 30% cover, both boards show f -Re relations with positive curvature across the six highest flow rates. However, the Moody plots, especially for the flat board (Figure 5), are remarkably flat overall, with only a mild concave-upward form.

This progressive change in the f -Re relations with increasing obstacle cover suggests a related progressive change in the behaviour of the flow field. The accepted explanation for positively sloping f -Re relations in flows with emergent obstacles is that, as the flow rate increases, the obstacles provide an increasing upslope-projected area obstructing the flow. This 'projected-area hypothesis' has been widely cited (Abrahams *et al.*, 1986; Rauws, 1988; Gilley *et al.*, 1992; Abrahams and Parsons, 1994; Lawrence, 1997). However, it cannot account for the concave-upward relations found in the present experiments. No positive f -Re slopes were found for 10% obstacle covers, despite the upslope projected area rising with imposed flow. Likewise, the f -Re slopes remain negative for the 20% and even the 30% obstacle covers, at least at the lower flow rates. These negative slopes indicate the conventional decline in f with increasing Re that typifies laminar flow not obstructed by obstacles (White, 1999). The tendency for the f -Re relations to then flatten at higher flow rates in the 20% and 30% obstacle covers suggests that an opposing effect is developing in the flow, the two effects resulting in little net change in f with rising Re. The depth and tachometer data presented earlier suggest that this is, in fact, the progressive onset of flow controls at gaps among the obstacles. It appears that, progressively, narrow and then wider gaps begin to act as controls, and the tendency for f to fall with Re is offset by the creation of backwater regions whose properties (relatively deep but slow flow) result in the flow-field value of f beginning to rise. This effect becomes strongest at high flow rates and 30% obstacle cover. The onset of strong positive f -Re curvature also begins at a lower flow intensity on the flat board (about Re = 300) than on the channel board (about Re = 450). On the channel board, the flow is somewhat concentrated by the axial channel, leaving inactive some potential flow controls located beyond the channel. It is possible that a flattening of the f -Re slope, and even the onset of positive slope, might have been observed for 10% cover had higher imposed flow rates been employed. Further experimentation is needed to evaluate this possibility. An alternative is that obstacle submergence and a decline in hydraulic roughness arise at higher flow rates, with positive f -Re slope not being exhibited.

In the view of filament-and-backwater flow advanced here, the positive f -Re slope is explained not by growing upslope-projected obstacle area, but by the onset of hydraulic control by narrow gaps between obstacles. Some component of the rising f will also be contributed by the form drag arising from the increasing projected area. However, this seems likely to be a relatively minor cause of drag, since the flow lying upstream of many of the obstacles is slow-moving backwater flow, which could contribute only minor viscous dissipation. In the presence of flow filaments, there would be an additional source of drag arising from viscous losses in mixing zones between filament- and backwater-flow zones. Furthermore, at narrow gaps, the flow may become turbulent, and further increase viscous dissipation. Thus, the flow filaments and the flow controls appear to be the loci of viscous dissipation, not the zones where flow is obstructed by the upstream faces of the obstacles.

For 30% cover, the total upstream-facing obstacle width for layouts A-E (and hence the upstream area, for any for depth) is, in fact, relatively uniform, all having between 100 and 130 cm of width. Thus, it appears that the significantly different values of f exhibited by these arrangements (differing by several hundred percent) cannot be accounted for in terms of differing upslope-projected wetted area, and that, therefore, this parameter cannot, for instance, account for the much higher f arising with layout A than with layouts B or E.

No comparably simple geometric measure can be expected to account for the complex filament-and-backwater flow phenomena causing positive f -Re slopes, since such a flow field involves multiple controls, filaments, and backwater zones. However, layout A (highest f at 30% cover on flat and channel boards) has two narrow gaps at the bottom end of the obstacle field, which the depth and velocity data suggest act as hydraulic flow controls at higher imposed discharges. On the other hand, layouts B and E (lowest f at 30% cover) both have much more open obstacle layout in this area, permitting readier passage of the imposed flow. Layout C, which provided a value of f not much below that of layout A, exhibits a relatively restricted set of flow paths, with the top right corner of the obstacle field in particular having no free paths to pass

downslope flow. Significant backwater effects would thus be anticipated for layout C, and, therefore, deeper backwater flows, consistent with the derivation of high f values for this layout.

This analysis leads to the conclusion that positively sloping f -Re relations may be partly, perhaps dominantly, an artefact of the use of flow-field mean properties. According to the calculations presented above, a single flow filament can carry 40% of the total flow, and the obstacle fields tested were crossed by two or three flow filaments. Although strict boundaries for filaments (or backwaters) are difficult to define (and, indeed, may involve gradational changes in flow properties), it seems reasonable to conclude that for largely laminar flows, as tested here, and in conditions where the f -Re relations exhibit positive slope, most flow is carried in filaments and only a small proportion is carried in the backwater zones. Since they have very different depths and velocities, similarly different friction coefficients would apply to filaments and backwaters, as shown earlier, if not concealed in a flow-field mean.

This raises the issue of whether the estimation of a flow-field friction coefficient ought to weight observations made in the two zones equally. This is the basis for the conventional method of deriving estimates of f using regularly spaced observations of flow depth and the calculation of a single mean depth and velocity for the flow field, or multiple measurements of velocity on separate dye tracks and the calculation of a single flow-field mean depth. However, if indeed most of the flow is carried in filaments, then it may be that, for practical purposes, the value of f ought to be discharge-weighted. This was suggested for the calculation of friction coefficients for streamflow by Lewis (1997), using similar reasoning. Evidently, from the results described earlier, the mean of the grid-based gantry depth measurements used to estimate mean velocity from $v = Q/wd$ reflected the areal dominance of deep, relatively slow-moving backwater areas, the narrower and faster filament flows being under-represented owing to their smaller areal extent. Thus, the Darcy-Weisbach friction coefficients derived for these flows were weighted according to backwater and filament *areas*, and not by the flow actually conveyed within them. If this interpretation is correct, then equally spaced depth readings collected on cross-sections of the flow will not provide an appropriate data source, however densely the observation points are set out.

The 15 tachometer velocity measurements show that several filaments of flow cross the obstacle field in layout A (which yielded the highest f value among the five layouts) while maintaining mean velocities of twice the flow-field mean. Even the slowest flow recorded anywhere along the flow filaments on the flat board exceeded the flow-field mean. This was a profile-mean of 4.9 cm s^{-1} recorded at point I, where the flow filament was in fact travelling *up* the slope of the board against the gradient. The fast filament velocities are sustained despite the most sinuous of the paths involving a total flow length of 90 cm in crossing the 50 cm straight line downslope width of the obstacle field, including the section where flow was upslope. Thus, the filaments may have an effective gradient considerably less than the board-slope of 1.2. It is customary to assume that a single slope applies to the whole flow-field, but this also may not be a close approximation to the actual situation in non-uniform flows.

An interesting point is the apparent difference between flow filaments produced by microtopography and those created by the positions of gaps between obstacles. The former are deeper and faster than the non-filament areas, whereas the latter are often shallower and faster than the backwater areas of the flow field. However, for filaments passing between obstacles that are acting as controls (i.e. at sufficiently high arriving discharges) the depth is rapidly variable in the vicinity of the gap itself. There is commonly significant deepening just above the constriction of flow, and then a rapid drop, perhaps to critical flow with maximum specific energy, as the flow passes through the constriction (Henderson, 1966; White, 1999). Moreover, the distribution of flow depths in regions of positive f -Re curvature (Figure 9) are not bimodal, so that almost certainly the flow depths change gradationally between filament and backwaters flows. This means that recognizing these two zones of the flow is itself only an approximate description of the complex non-uniform flow field.

It is worth emphasizing here that the obstacle cover fractions employed in the present experiments lie within the range of surface stone covers widely reported from dryland areas globally. Therefore, it can be inferred that surface runoff on such stony slopes involves hydraulic flow controls created by closely spaced stones obstructing flows. Thus, in major runoff events, when these flow controls were operating, relatively deep backwater areas would develop, with flow filaments crossing them at greater velocity. Under these conditions, friction coefficients based upon scattered depth measurements may not adequately reflect the conditions of the

non-uniform flows. It is hypothesized that the same kind of filament-and-backwater flow behaviour would be developed in surface runoff on a soil surface carrying large detritus from harvested crop residue, or coherent clods resulting from tilling operations. Thus, flows of the kind analysed may be widespread in a range of environments. For obstacle distributions more uniform than the random ones tested here, however, the effects may vary from those reported earlier. Additional experimentation is needed to explore these conditions.

The recognition of filament-and-backwater flow potentially has significance beyond the immediate issue of calculating friction coefficients. Evidently, flow filaments will have much higher velocities, and so a higher competence to entrain and/or carry soil particles. Concealing the existence of such zones in a flow-field mean value of f lowered by backwater effects seems undesirable. The high sediment transport competence of filament flows occupying a small fraction of the surface area, but under-represented in evenly spaced depth observations, could then result in unaccountably high sediment yields in erosion plot studies. For reasons such as this, it may prove desirable to recognize the existence of flow filaments, and to adopt methods for observing flows and processing the resulting data that yield independent information on backwater areas as well as on faster flow filaments. The optical tachometer developed for this work provides a convenient means to measure flow velocities independently of depths. Finally, the development of relatively deep backwater areas might also be of significance in soil entrainment, since splash effects are modified by the thickness of surface water films.

CONCLUSIONS

The experiments with obstacle fields on both the flat and channel boards showed that friction coefficients depend strongly on obstacle layout. Thus, in the study of flow on stony desert hillslopes, and by analogy through crop residues, simple cover fraction appears not to provide a sufficiently sensitive measure of an obstacle field. Moreover, the results showed that friction coefficients are modified by the presence of micro-topography. At obstacle cover fractions of $>10\%$ the channel board yielded friction coefficients lower than those of the flat board, but with a more marked upward-concavity of the f - Re relation. Thus, in accounting for the properties of flow in obstacle fields, both the geometric layout of the obstacles and the form of the surface beneath are significant. Similar conclusions were drawn by Takken and Govers (2000) in a laboratory study of flow across rough soil surfaces.

The collection of independent 'spot' readings of flow depth and velocity allowed the internal variability of flow conditions within the obstacle fields to be resolved. The results demonstrated that for 20 and 30% obstacle covers, and especially for the higher imposed discharges, flow-field friction coefficients rise with imposed flow rate. However, the results make it clear that this is not dominantly a function of the rising upslope-projected obstacle area causing viscous dissipation in the flow. Rather, the independent depth and velocity data showed that, under such conditions, the flow field contains both fast-moving flow filament and relatively sluggish backwater zones. Flow filaments were shown to carry the bulk of the discharge, and at flow velocities well in excess of the flow-field mean. Their depth is also less than that of backwater zones. The use of flow-field means for depth and velocity conceals the existence of these potentially important features of non-uniform flow. The results demonstrated that positively sloping f - Re relations arise at least partly from the method of data collection and averaging. If flow filaments are narrower than backwater zones, then they will be under-represented in depth data, flow-field velocities will be under-estimated, and friction coefficients over-estimated. Thus, conventional data in fact yield area-weighted flow properties. It may be that discharge-weighted flow properties would be of greater benefit in studies of surface hydraulics and of soil entrainment and transport, and procedures for deriving such values need to be developed.

ACKNOWLEDGEMENTS

I thank Peter Domelow and David Tooth, workshop technicians at Monash University, for their skilled help in the fabrication of apparatus. The work was supported by funding from the Australian Research Council.

REFERENCES

- Abrahams AD, Parsons AJ. 1990. Determining the mean depth of flow in field studies of flow hydraulics. *Water Resources Research* **26**: 501–503.
- Abrahams AD, Parsons AJ. 1994. Hydraulics of interrill overland flow on stone-covered desert surfaces. *Catena* **23**: 111–140.
- Abrahams AD, Parsons AJ, Luk S-H. 1986. Resistance to overland flow on desert hillslopes. *Journal of Hydrology* **88**: 343–363.
- Abrahams AD, Gao P, Aebly FA. 2000. Relation of sediment transport capacity to stone cover and size in rain-impacted interrill flow. *Earth Surface Processes and Landforms* **25**: 497–504.
- Barros AP, Colello JD. 2001. Surface roughness for shallow overland flow on crushed stone surfaces. *Journal of Hydraulic Engineering* **127**: 38–52.
- Dunkerley DL. 2001. Estimating the mean speed of laminar overland flow using dye injection – uncertainty on rough surfaces. *Earth Surface Processes and Landforms* **26**: 363–374.
- Dunkerley DL. 2002a. Volumetric displacement of flow depth by obstacles, and the determination of friction factors in shallow overland flows. *Earth Surface Processes and Landforms* **27**: 165–175.
- Dunkerley DL. 2002b. Surface tension and friction coefficients in shallow, laminar overland flows through organic litter. *Earth Surface Processes and Landforms* **27**: 45–58.
- Dunkerley DL. In press. An optical tachometer for short-path measurement of flow speeds in shallow overland flows: improved alternative to dye timing. *Earth Surface Processes and Landforms*.
- Dunkerley DL. 2003. Volumetric displacement of flow depth by obstacles in interrill flows: quantification using a new method applied to stone-mantled desert hillslopes at Fowlers Gap, New South Wales, Australia. *Water Resources Research*: submitted for publication.
- Dunkerley DL, Domelow P, Tooth D. 2001. Frictional retardation of laminar flow by plant litter and surface stones on dryland surfaces: a laboratory study. *Water Resources Research* **37**: 1417–1424.
- Dunne T, Dietrich WE. 1980. Experimental investigation of Horton overland flow on tropical hillslopes. *Supplementband Zeitschrift für Geomorphologie* **35**: 60–80.
- Emmett WW. 1970. *The Hydraulics of Overland Flow on Hillslopes*. US Geological Survey Professional Paper **662-A**. USGS: Washington, DC.
- Freund JE. 1974. *Modern Elementary Statistics*. Prentice-Hall.
- Gilley JE, Kottwitz ER, Wieman GA. 1991. Roughness coefficients for selected residue materials. *Journal of Irrigation and Drainage Engineering* **117**: 503–514.
- Gilley JE, Kottwitz ER and Wieman GR. 1992. Darcy–Weisbach roughness coefficients for gravel and cobble surfaces. *Journal of Irrigation and Drainage Engineering* **118**: 104–112.
- Henderson FM. 1966. *Open Channel Flow*. Macmillan: New York.
- Lawrence DSL. 1997. Macroscale surface roughness and frictional resistance in overland flow. *Earth Surface Processes and Landforms* **22**: 365–382.
- Lewis NK. 1997. Use of the discharge-weighted average velocity in studies of the frictional energy loss of streamflow. *Earth Surface Processes and Landforms* **22**: 329–336.
- Rauws G. 1988. Laboratory experiments on resistance to overland flow due to composite roughness. *Journal of Hydrology* **103**: 37–52.
- Roels JM. 1984. Flow resistance in concentrated overland flow on rough slope surface. *Earth Surface Processes and Landforms* **9**: 541–551.
- Takken I, Govers G. 2000. Hydraulics of interrill overland flow on rough, bare soil surfaces. *Earth Surface Processes and Landforms* **25**: 1387–1402.
- Weast RC (ed.). 1979. *CRC Handbook of Chemistry and Physics*, 60th edition. CRC Press: Boca Raton.
- Weltz MA, Arslan AB, Lane LJ. 1992. Hydraulic roughness coefficients for native rangelands. *Journal of Irrigation and Drainage Engineering* **118**: 776–790.
- White FM. 1999. *Fluid Mechanics*, fourth edition. McGraw-Hill: Singapore.